Journal of Molecular Liquids 390 (2023) 123100

Contents lists available at ScienceDirect

Journal of Molecular Liquids

journal homepage: www.elsevier.com/locate/molliq

Bent-core liquid crystals joining the ethylene-oxide/lithium ion tandem: Ionic conductivity and dielectric response towards new electrolytes for energy applications

Alfonso Martinez-Felipe [a,b,*], Daniel Zaton [a,c], Martín Castillo-Vallés [d], Asia Baldini [a,e], Jonathan Pease [a], Natalie Leader [a,1], Nurul Fadhilah Kamalul Aripin [f,g], Marco Giacinti-Baschetti [e], M. Blanca Ros [d,*]

[a] Chemical Materials and Processes Group, School of Engineering, King's College, University of Aberdeen, Aberdeen AB24 3UE, Scotland, UK
[b] Just Transition Lab, University of Aberdeen, Aberdeen AB24 3UE, Scotland, UK
[c] Department of Chemistry, School of Natural and Computing Science, Meston Walk University of Aberdeen, Aberdeen AB24 3UE, Scotland, UK
[d] Universidad de Zaragoza, Instituto de Nanociencia y Materiales de Aragón, Departamento de Química Orgánica, Facultad de Ciencias, Universidad de Zaragoza-CSIC, Campus San Francisco, E-50009 Zaragoza, Spain
[e] Department of Civil, Chemical, Environmental, and Materials Engineering, Università degli studi Bologna, Via Terracini 34, 40131 Bologna, Italy
[f] School of Chemical Engineering, College of Engineering, Universiti Teknologi MARA, 40450 Shah Alam, Selangor, Malaysia
[g] Department of Chemistry, School of Natural and Computing Sciences, University of Aberdeen, King's College, Aberdeen AB24 3UE, Scotland, UK

ARTICLE INFO

Keywords:
Bent-core liquid crystals
Ionic conductivity
Dielectric analysis
Energy conversion and storage
Fourier-transform infrared spectroscopy

ABSTRACT

We report the dielectric and conductivity response of three materials containing bent-core and tetra(ethylene-oxide) moieties, and their complexes doped with lithium triflate salts, as new potential nanostructured electrolytes. Whilst the pristine bent-core compounds do not show mesomorphism, the doped materials display smectic mesophases inside indium tin oxide cells assisted by the selective solvation of the lithium ions in the ethylene-oxide blocks. The dielectric response of the materials in the high-frequency range is controlled by the chemical composition of the bent-core structure, and the presence of lithium ions promotes direct current conductivity at low frequencies, in the $\sigma_{dc} \sim 10^{-5}$ S cm^{-1} range, which can be enhanced to $\sigma_{dc} \sim 10^{-4}$ S cm^{-1} via *trans*-to-*cis* photoisomerization of azobenzene groups. The dynamic and dual character of these materials (responding to low and high frequency electrical fields), the formation of ferroelectric crystals capable to store energy, and their interactions with light, will be applied to develop new energy devices.

1. Introduction

The preparation of new solid or quasi-solid organic electrolytes with high ion conductivities will accelerate the development of more efficient energy devices, such as, batteries, fuel cells, or energy harvesters and will ultimately contribute to achieve net-zero targets [1,2]. Thermotropic liquid crystals (LCs) form fluid mesophases that retain different degrees of orientational (and potentially positional) order as a function of the temperature, offering exciting possibilities for technological applications [3–5]. Liquid crystals have created high expectations for generation of new 1D, 2D and 3D dynamic nanostructured materials for energy applications, by using classic columnar, smectic and bicontinuous cubic mesophases respectively, and the manipulation of their orientation [6,7]. The formation of micro-segregated regions with molecular mobility, for example, can facilitate ionic transport, and the response of liquid crystals to electrical fields and macroscopic polarisation can be particularly advantageous in electrochemical devices and flexible electronics [8]. The presence of dipoles and cooperative motions in liquid crystalline phases result in a variety of responses to electrical fields, which can be study by dielectric spectroscopy [9].

Bent-core liquid crystals (BCLCs) [10–16] were discovered in the mid 1990's [17] and rapidly attracted interest due to their ferroelectricity

* Corresponding authors at: Chemical Materials and Processes Group, School of Engineering, King's College, University of Aberdeen, Aberdeen AB24 3UE, Scotland, UK (A. Martinez-Felipe).
E-mail addresses: a.martinez-felipe@abdn.ac.uk (A. Martinez-Felipe), bros@unizar.es (M. Blanca Ros).
[1] Natalie Leader. Xodus Academy Xccelerator, 50 Huntly Street AB10 1RS, Scotland, UK.

https://doi.org/10.1016/j.molliq.2023.123100
Received 18 June 2023; Received in revised form 12 September 2023; Accepted 16 September 2023
Available online 17 September 2023

(even when composed by achiral molecules) that can be tuned by the application of electrical fields leading to interesting functional materials [18]. Their capability to yield permanent polarisation within layers or columns is based on the presence of dipoles in their molecular structures and the formation of compact packing arrangements that restrict rotational freedom. BCLCs can exhibit a variety of mesophases including polar smectic A (SmAP) and smectic C (SmCP, former B_2), dark conglomerate (DC) [19], columnar (Col, former B_1), helical nanofilaments (HNF) [14,20], frustrated lamellar [10] and the recently discovered twist-bend nematic [21–23]. Interest in finding new liquid crystalline ferroelectric and conducting materials continues to grow, and extends towards other molecular geometries capable to exhibit local symmetry breaking, including polar calamitic nematic LCs [24–27].

In our precedent work, we described the synthesis and characterisation of a series of new amphiphilic BCLCs containing lithium triflate ions [28]. Our materials comprise one hydrophilic tetra(ethylene-oxide) chain broadly identified as tetra(ethylene glycol) [TEG], covalently linked directly to a hydrophobic part formed by a C_{14}-alkoxy tail and a bent-core (BC) containing five aromatic rings, see Fig. 1. Three different connections have been considered for the lateral cores of the BC structures: a common ester linking group (B1), broadly used in our previous studies (compound TEG-B1-0-14); the straight union *via* a biphenyl (Bi) moiety, inspired by the trend of biphenyl lateral cores to promote the HNFs mesophase formation (compound TEG-Bi-0-14); and an azo linker (Bazo) in order to obtain photoresponsive materials (compound TEG-Bazo-0-14).

Herein, we will investigate the potential of our bent-core based materials as electrolytes for energy conversion and storage devices. Lithium ion-conductive liquid-crystalline (LC) electrolytes containing oligo(ethylene-oxide)s have been already proposed for battery applications, based on their capacity to host ionic charges in ordered morphologies [29–39]. Kato and co-workers, for example, have studied the formation of layered microstructures in a series of liquid crystalline materials, with emphasis on their potential for high-oxidation-resistance [4,6,40–42]. The formation of smectic phases in ionic liquid crystals containing lithium bistriflimide salts has been also suggested by our own group [43], and, more broadly, ionic liquids with controllable channels have been recently investigated [44–46]. Interestingly, and despite their advantageous structural features, bent-core liquid crystals remain mostly unexplored as conducting materials [47–50], and we intend to investigate the functionality of our materials in this work. We will first present a dielectric study of the non-doped materials, TEG-B*x*-0-14, to determine relevant compositional aspects, and we will then correlate the conductivity of the doped samples (Li-TEG-B*x*-0-14) with their chemical structure and phase structure. The presence of the azobenzene group, as in TEG-Bazo-0-14 and Li-TEG-Bazo-0-14, introduces interesting packing abilities in bent-core mesophases [51] and the exciting possibility to control the dielectric response and conductivity by the application of light [52–59], and this will be preliminarily studied here. Our aim is to assess the potential of these and related materials in future energy devices.

2. Materials and techniques

Six materials are studied in this work (Fig. 1). The synthesis and physic-chemical characterisation of the three bent-core compounds, namely, TEG-B1-0-14, TEG-Bi-0-14, and TEG-Bazo-0-14, are described in detail in a precedent work, and are summarised as supplementary information [28]. The Li-doped samples were prepared at room temperature by mixing THF solutions of the corresponding undoped TEG-B*x*-0-14 compounds (1 M) and lithium triflate (1 M) by sonification during 15 min, followed by solvent evaporation under stirring, and further drying in a desiccator for 24 h. This process yielded three solid complexes with 1:1 M ratios of Li ions to bent-core compounds, labelled as Li-TEG-B*x*-0-14. Whilst the pristine bent-core compounds do not show mesomorphic properties and crystallise directly from the melt, complexation with lithium induces liquid crystalline behaviour. More specifically, Li-TEG-B1-0-14 develops a Smectic C polar phase (SmCP) between 92 °C, and 60 °C, and Li-TEG-Bi-0-14 and Li-TEG-Bazo-0-14 induce helicoidal nanofilaments-like mesophases (HNFs) below 98 °C and 90 °C, respectively, prior to crystallisation. The phase behaviour of these compounds is discussed in detail in our precedent publication [28] and summarized as electronic supplementary information, ESI.

The dielectric response and conductivity of the materials were assessed in transparent cells between parallel electrodes. A few milligrams of the samples were introduced in the melt state by capillary action inside Indium Tin Oxide cells, ITO (SG100A080uG180, Instec), containing polyimide coatings to yield anti-parallel alignments with 1° to 3° pre-tilted angles. Cells have active areas of $A = 100mm^2$, with 100 Ω resistance and $\nu = 8$ μm thickness, and the cell capacitance is then calculated as,

$$C_O = \varepsilon_O \frac{A}{\nu} = 1.10675 \cdot 10^{-10} F$$

where $\varepsilon_O = 8.854 \cdot 10^{-12} F \cdot m^{-1}$ is the dielectric permittivity of vacuum.

We have assessed the phase behaviour of the materials in the ITO devices by polarised optical microscopy (POM), using an Olympus BH-2 microscope, with the temperature controlled by a Linkam THMS 600 heating stage and TMS 91 control unit (±0.1 K). Interestingly, as we will show later, the phase transitions of the hybrid materials are modified with respect to those established by DSC, although with a repetitive character, when the materials are introduced into the ITO cells. This is attributed to different surface effects on the organization of the fluid material and to be materials with a variable organic-cation molecular interaction.

We have carried out additional Fourier-transform infrared spectroscopy measurements (FT-IR), to determine short-range interactions

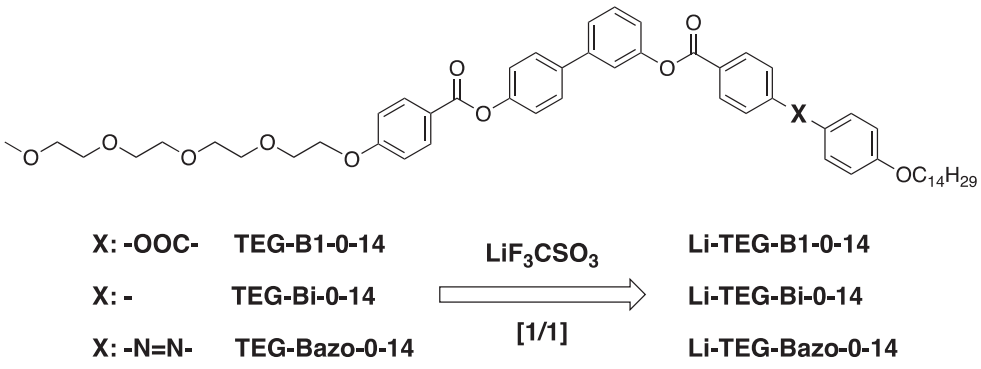

Fig. 1. Chemical structure of the bent-core compounds, TEG-Bx-0-14, and the lithium triflate ionic group used to yield the lithium complexes under study, Li-TEG-Bx-0-14.[28].

involving different functional groups in the molecular segments of the materials. The FT-IR spectra were obtained using a Thermo Nicolet NEXUS 470 FT-IR spectrometer with 4 cm^{-1} resolution in the 4000–400 cm^{-1} range, as the average of 64 scans, and analysed with OMNIC software, using the Linkam THMS 600 hot stage for temperature control (±0.1 °C). Measurements were taken in transmission mode with the samples sandwiched between two KBr windows.

The dielectric and conductivity response of the materials in the cells was studied by complex impedance spectroscopy, in terms of their complex dielectric permittivity,

$$\varepsilon^* = \varepsilon' - i\varepsilon'' \quad (1)$$

where ε' is the dielectric elastic constant, ε'' the loos factor, and i the complex unity, and the complex conductivity,

$$\sigma^* = \sigma' + i\sigma'' \quad (2)$$

where σ' and σ'' are the real and imaginary components, respectively. The dielectric permittivity and conductivity can be related by,

$$\sigma^* = i\omega\varepsilon_0\varepsilon^* \quad (3)$$

where ω is the angular frequency of the alternating electrical field.

The ITO cells were connected to a PARSTAT MC multichannel potentiostat (Ametek) on a Linkam TMS 91 hot stage for temperature control (±0.1 °C). The dielectric measurements consisted of isothermal frequency sweeps between 10^6 Hz and 0.1 Hz, with V_{rms} = 1000 mV amplitude alternating electric fields, and the majority were taken in the absence of bias electric fields (V_{bias} = 0 V). Experiments were carried out by cooling from the isotropic phase to room temperature in 2 °C isothermal steps, allowing for thermal equilibrium before measuring.

Additional measurements were performed on the samples containing azobenzene groups (TEG-Bazo-0-14 and Li-TEG-Bazo-0-14), to evaluate the effect of UV light on their dielectric and conductivity response. To do that, we irradiated the corresponding cells with a fixed intensity of 260 mW cm^{-2}, using a Dymax ACCU-CALTM 50-LED at 365 nm, and carried out simultaneous measurements under alternating electrical fields using the PARSTAT potentiostat with the same configuration as described above. The intensity was measured with a UV light detector, located at the same distance from the light source as the Linkam THMS 600, using a colour filter to remove the UV light from the microscope's light source. The UV–vis spectra of the azobenzene-containing compounds were collected for tetrahydrofuran, THF, solutions (10^{-5} M). Samples were irradiated with UV light (365 nm, 260 mW·cm^{-2}), and the UV–visible spectra were obtained as a function of exposure and relaxation time, using a VARIAN Cary 50 Scan UV–vis spectrophotometer, between 300 nm and 550 nm. Additional ferroelectric measurements on non-doped samples were carried out by a RT66C Test System (Radiant Inc), by measuring the polarisation of the cells at different temperatures, through hysteresis loops of sinusoidal fields in the ± 10 kV range, and at several frequencies.

3. Phase behaviour and short-range interactions

As mentioned above, whilst the non-doped bent-core compounds, TEG-B*x*-0-14, do not show mesomorphic behaviour and crystallise on cooling from their isotropic melts, the three lithium-doped materials, Li-TEG-B*x*-0-14, develop liquid crystalline phases in the ITO cells as seen under POM. As discussed before, different phase behaviour and transition temperatures were observed for the materials inside the ITO cells on cooling from their melts, as is summarized in Table 1, and selected textures are depicted in Fig. 2.

Li-TEG-B1-0-14 develops birefringent regions at high temperatures with four-point disclinations on a stripped black background, Fig. 2**(a)**, which evolve on cooling to a grain-like texture, Fig. 2**(b)**. Li-TEG-Bi-0-14 displays a focal fan structure at high temperatures (T < 149 °C), Fig. 2 **(c)**, which develops into a less defined texture on further cooling, Fig. 2 **(d)**, but without an apparent phase transition. We note that these are different from the HNF textures observed between non-treated glasses, normally less birefringent and difficult to assign [28]. Li-TEG-Bazo-0-14, on the other hand, shows well-defined stripes in a broad range of temperatures below 146 °C, Fig. 2**(e)**, before developing a granular texture below T ~ 107 °C, Fig. 2**(f)**. The textures in Fig. 2 are consistent with the formation of smectic phases, suggesting that strong surface effects in the measuring cells can disrupt and inhibit the order needed to form HNF-like phases. In the absence of other experimental data, it is confirmed that all Li-based materials in ITO cells form smectic-type mesophases, which are assigned as an unidentified mesophase (M). The liquid crystal order is highly responsive to boundary conditions to yield orientational structures, and the application of rubbed surfaces can lead, for example, to planar polar preferential alignments, and this also could be expected for bent-core phases. [60] It is also worth noting that we did not observe phase transformations under the application of moderate electrical fields (≤ 3 V), suggesting that the phase structures are stable under these conditions.

Table 1
Summary of the phase behaviour observed under POM on cooling the bent-core compounds (−10 °C·min^{-1}) inside the ITO cells. All temperatures in °C.

Bent-core compounds		Li-doped bent-core compounds	
TEG-B1-0-14	I – 74 – Cr	Li-TEG-B1-0-14	I –128 – M – 84 – Cr
TEG-Bi-0-14	I – 103 – Cr	Li-TEG-Bi-0-14	I –149 – M – 92 – Cr
TEG-Bazo-0-14	I – 90 – Cr	Li-TEG-Bazo-0-14	I –146 – M –107– Cr

I: Isotropic phase; M: unidentified mesophase, tentatively assigned as smectic-type phase based on POM textures; Cr: crystal.

The smectic phases in the Li-TEG-B*x*-0-14 samples can be the result of microphase separation between polar and non-polar segments (amphiphilic character), which is further enhanced by complexation with the lithium triflate salt. In Fig. 3 we compare the Fourier-transform infrared spectra, FT-IR, of the azobenzene-based materials (TEG-Bazo-0-14 and Li-TEG-Bazo-0-14) at similar temperatures. In the high-mid frequency region, the spectra depict signals associated to stretching (ν) vibrations of aromatic (>3000 cm^{-1}) and aliphatic (<3000 cm^{-1}) groups, contributions from the –COO- groups (1730 cm^{-1}) and aromatic ring vibrations (1600–1500 cm^{-1}) [61]. At lower frequencies, several strong bands appear between 1350 and 1000 cm^{-1} associated to the $–CH_2$-O-CH_2- groups at the TEG tails of the molecules, together with some signals related to aromatic C–H vibrations at the bent-core segments (784 cm^{-1} and 865 cm^{-1}). As expected, all samples show similar FT-IR spectral features based on their molecular similarities, see **Fig. ESI1**.

In the doped samples, Li-TEG-B*x*-0-14, the 1350 cm^{-1} and 1000 cm^{-1} regions undergo several changes due to complexation of lithium triflate to the TEG chains, and some new bands appear associated to the triflate ion. A prominent peak is seen near 650 cm^{-1}, related to bending of the sulfonic group $\delta(SO_3)$, together with new signals around 1310 cm^{-1}, where the stretching vibrations of the -CF_3 (symmetric, ν_s) and -SO_3 (asymmetric, ν_a) groups are expected, and a new shoulder at around 1045 cm^{-1}, associated to the symmetric stretching vibration of the sulfonate group, $\nu_s(SO_3)$ [62–64]. The main bands attributed to the ethylene-oxide units in the TEG chains (1254, 1206, 1168, 1137, and 1067 cm^{-1}) broaden in the lithium-containing samples, and seem to split into several contributions [65]. These are clear signs of new interactions typical of cooperative molecular systems, such as oligomers and polymers, where the relaxation time-constant is higher, and confirm that the lithium triflate species are located, at least preferentially, in the TEG segments of the molecules. As a result, the higher polarity around the TEG segments, with polar nature, promotes microphase separation respect to the non-polar bent-core ones, and ultimately facilitates the formation of smectic phases. Furthermore, these results are in good agreement with the parameters estimated by XRD for their mesophases, and what was proposed in our previous article [28], as well as with the

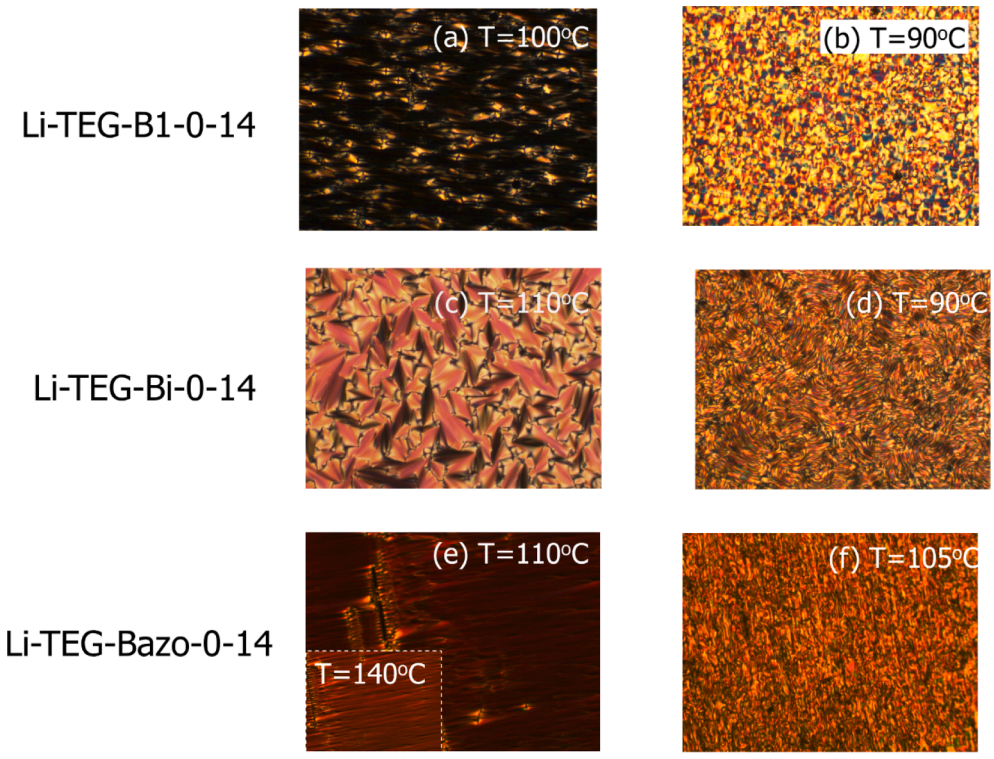

Fig. 2. Polarised optical micrographs of the bent-core compounds obtained on cooling from their melts, inside the ITO cells, showing birefringent regions at different temperatures: Li-TEG-B1-0-14 (a, b); Li-TEG-Bi-0-14 (c, d); Li-TEG-Bazo-0-14 (e, f).

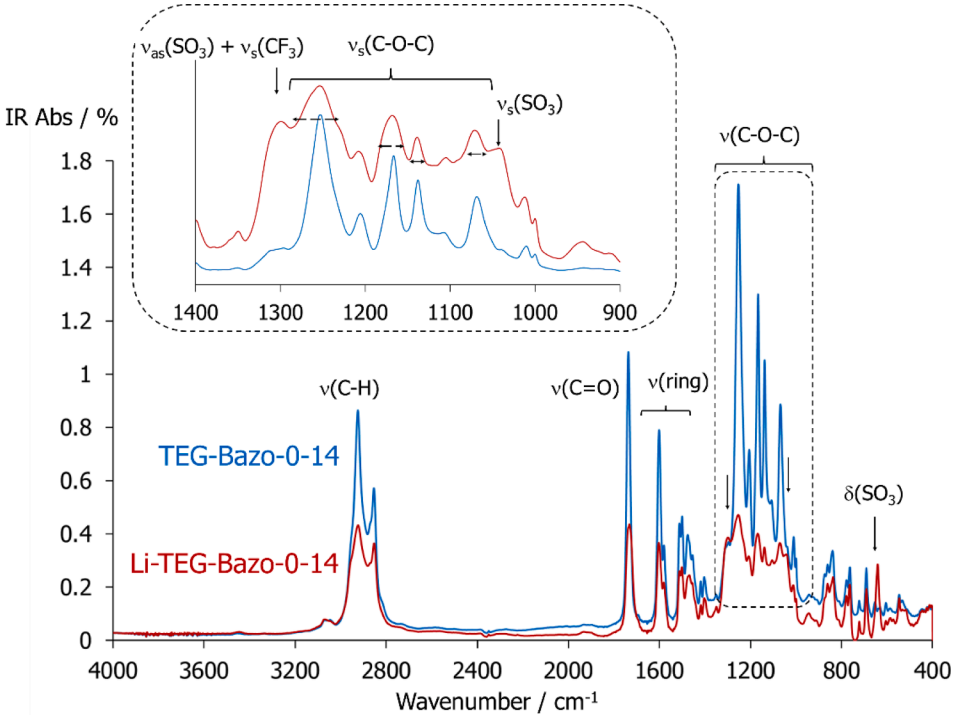

Fig. 3. FT-IR spectra corresponding to TEG-Bazo-0-14 (blue) and Li-TEG-Bazo-0-14 (red) measured at T = 104 °C (in KBr). Selective complexation of the lithium triflate ions in the TEG region is assessed by the appearance of new contributions from the triflate ions (vertical arrows) and broadening of the C-O-C stretching bands (dotted horizontal arrows in the inset). (For interpretation of the references to colour in this figure legend, the reader is referred to the web version of this article.)

widely proved idea that the microsegregation of incompatible molecular segments in different domains is the main driving force of liquid crystalline self-organization [66].

4. Dielectric and conductivity response

4.1. Non-doped compounds: TEG-Bx-0-14 series

Prior to investigating the lithium-doped bent-core compounds, we now study the dielectric and conductivity response of the three non-doped materials, TEG-B*x*-0-14.

The isothermal ε'' Bode plots as a function of the frequency obtained on cooling steps are summarised in Fig. 4, and the corresponding ε' Bode plots are shown as **Fig. ESI2**. All the non-doped samples show a prominent and sole ε'' peak with maxima (ε''_{max}) in the mid-frequency region ($\sim 10^1$ to 10^4 Hz), appearing by reorientation of the dipoles in the molecules under the weak alternating fields ($\pm$ 1 V_{rms}). Since the peaks shift to lower frequencies on cooling, see for example Fig. 4**(a)** for TEG-Bi-0-14, these ε'' processes can be ascribed to dielectric relaxations that require longer relaxation times, $\tau = 1/f$, at lower temperatures. The sudden drop in ε'' observed for TEG-B1-0-14 in Fig. 4**(b)** must be attributed to crystallisation in the cell (T < 84 °C).

We have studied the temperature dependence of the dielectric relaxations in Fig. 4, by obtaining the frequencies, *f*, at which the peak maxima appear, ε''_{max}, and preparing the corresponding Arrhenius plots, **Fig. ESI3**,

$$\ln\left(f_{\varepsilon''_{max}}/Hz\right) = \ln(f_0) - \frac{E_a}{R}\frac{1}{T} \quad (4)$$

where, E_a is the activation energy, and $\ln(f_0)$ a pre-exponential factor. The linear profiles and E_a values calculated (~40 kJ mol^{-1}, see Table 2) are typical of locally activated processes, and are consistent with the energy barrier involved in the rotation of rod-like and bent-core molecules [67,68]. The almost coinciding activation energy values obtained for the three non-doped samples indicate the same molecular origin for the dielectric relaxation, which is expected due to their structural similarities, recall Fig. 1. We believe that the presence of two ester groups in all the three compounds contributing to the overall polarity of the rigid core may override the chemical (and polarity) difference of the linking groups ***X*** (benzoate, biphenyl, azobenzene structures).

In order to investigate the origin of this relaxation, we have remeasured the dielectric response of TEG-Bazo-0-14 (80 °C) while superimposing direct current (dc) fields (≤4V). The results, shown in **Fig. ESI4(a)**, indicate that this relaxation remains unaltered by the presence of dc fields, which is typical of local soft-modes, and is also consistent with the absence of liquid crystalline structures and the low activation energies depicted in Table 2 [69–71].

Table 2
Activation energies, E_a, and temperature intervals, T, corresponding to the main dielectric relaxation after fitting to Arrhenius behaviour.

Bent-core compounds			Li-doped bent-core compounds		
	E_a/ kJ·mol^{-1}	T interval/ °C		E_a/ kJ·mol^{-1}	T interval/ °C
TEG-B1-0-14	44	76/102	Li-TEG-B1-0-14	105	28/44
TEG-Bi-0-14	44	36/104	Li-TEG-Bi-0-14	95	28/66
TEG-Bazo-0-14	38	40/80	Li-TEG-Bazo-0-14	*	*

*Non-visible temperature dependence.

The high dielectric values displayed by the non-doped samples in Fig. 4 and **Fig. ESI2** must arise from local redistributions of charges under electrical fields, even in the absence of ions. We have then plotted in Fig. 5 the temperature and frequency dependence of the real component of the complex conductivity (σ') for the TEG-B*x*-0-14 series. At sufficiently high temperatures, the rise of ε'' observed at low frequencies is attributed to the existence of strong direct current (dc) conductivity between the electrodes, σ_{dc} [61], and this is confirmed by the plateaus in the σ' vs *f* double logarithmic plots. As expected, the dielectric response (ε'') at low frequencies also increases upon the application of the superimposed dc fields in **Fig. ESI4(a)**. The drop in the σ' values at low frequencies must be attributed to strong electrode and/or Maxwell/Wagner/Sillars polarization effects, due to the accumulation of charges on the electrode surfaces [72]. The corresponding σ_{dc} values were estimated by extrapolating the σ' curves to $f \rightarrow 0$ in Fig. 5, and these results will be further explored for the doped materials in the next section.

4.2. Li-Doped bent-core compounds: Li-TEG-Bx-0-14 series

We now study the dielectric and conductivity response of the samples doped with lithium triflate salts, and Fig. 6 displays the dielectric loss factor, ε'', obtained for the Li-TEG-B*x*-0-14 series. **Fig. ESI5** shows the corresponding dielectric elastic constant values, ε'. In the mid-high frequency region, the three doped samples show one dielectric relaxation with ε''_{max} values comparable to those reported above for the corresponding non-doped materials in Fig. 4. This is accompanied with

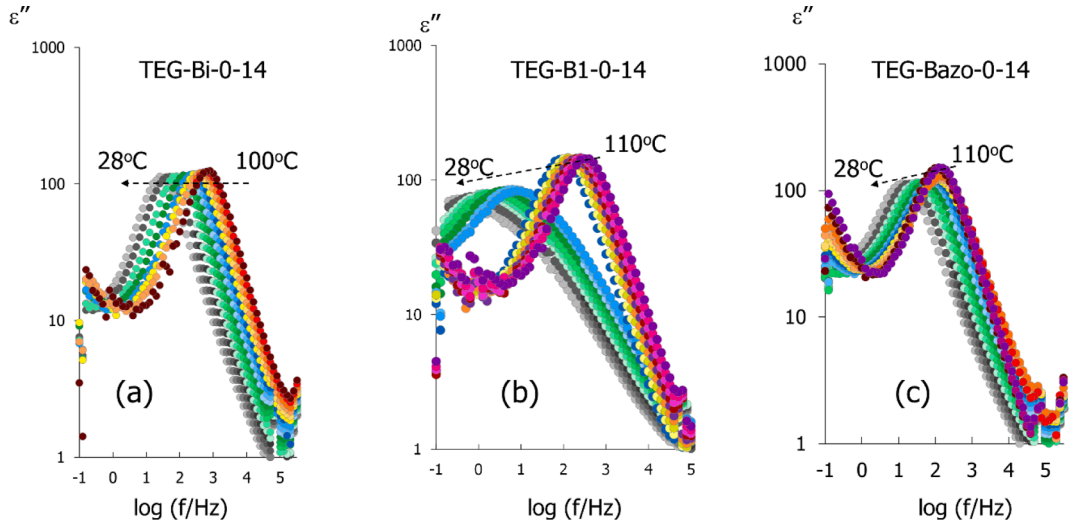

Fig. 4. Bode plots showing the frequency and temperature dependence of the dielectric loss factor, ε'', measured for the non-doped samples: (a) TEG-Bi-0-14, (b) TEG-B1-0-14, and (c) TEG-Bazo-0-14, on cooling from the corresponding isotropic melts. Arrows indicate direction on cooling.

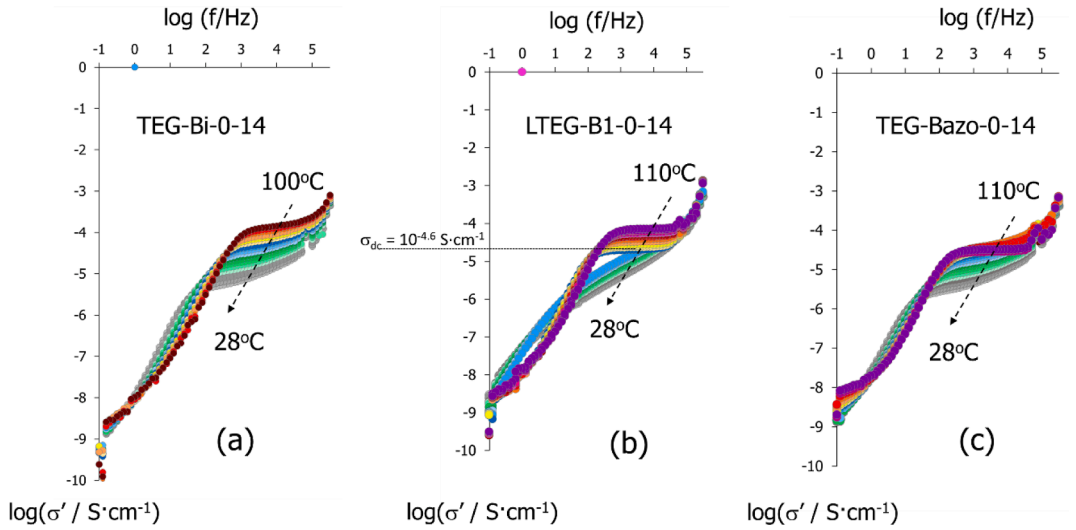

Fig. 5. Double logarithmic plots of the real component of the complex conductivity, σ′, measured as a function of the frequency, log(σ′) vs log(f), in isothermal steps (ºC) on cooling from the isotropic phases for: (a) TEG-Bi-0-14, (b) TEG-B1-0-14, and (c) TEG-Bazo-0-14. Estimation of DC conductivity, σ_{dc}.

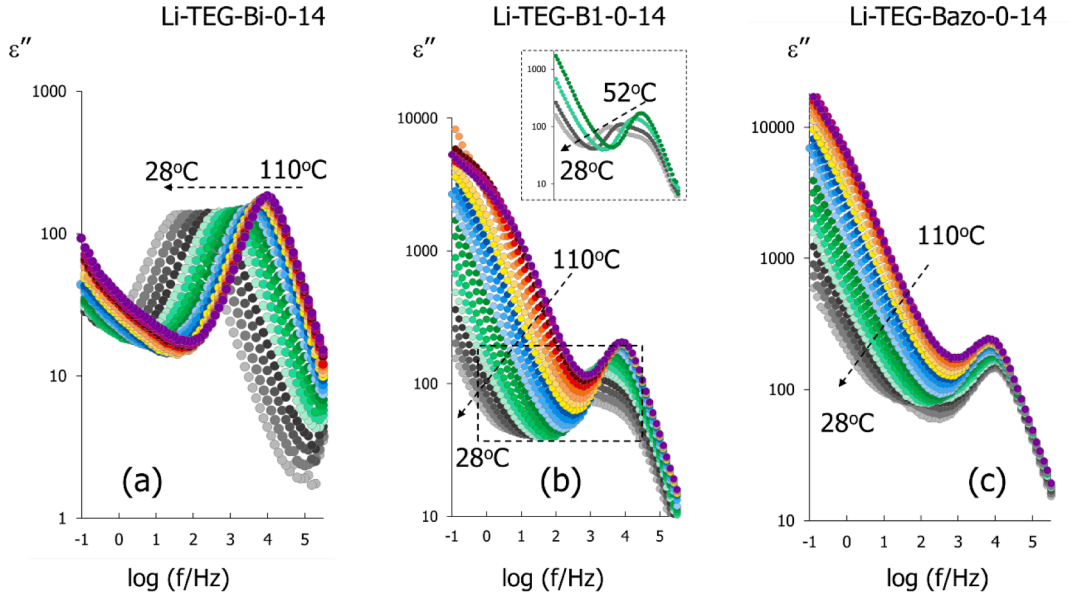

Fig. 6. Frequency and temperature dependence of the dielectric loss factor, ε″, measured for the Li-doped samples: (a) Li-TEG-Bi-0-14, (b) Li-TEG-B1-0-14, and (c) Li-TEG-Bazo-0-14, on cooling from the corresponding isotropic melts. Arrows indicate direction on cooling.

additional dielectric signals in the low-frequency end, which results in considerably higher ε″ values in the case of Li-TEG-B1-0-14 and Li- TEG-Bazo-0-14, Fig. 6**(b)** and Fig. 6**(c)**, respectively, compared to their corresponding non-doped analogous. We have obtained the maxima of the ε″ curves in Fig. 6 for the Li-doped samples, ε''_{max}, and the corresponding Arrhenius plots are shown in **Fig. ESI6**.

Interestingly, Li-TEG-Bi-0-14 displays in Fig. 6**(a)** and **Fig. ESI6(a)** a clear Vogel-Fulcher-Tamman behaviour, VFT, typical of polymers and viscous materials, which involves segmental or cooperative motions that depend on the free volume [73]. The maxima in the ε″ curves can be then fitted to the following expression,

$$\ln\left(f_{\varepsilon''_{max}}/Hz\right) = \ln(f_0) - \frac{B}{T - T_0} \quad (5)$$

where $\ln(f_0/Hz) = 10.6$ is a pre-exponential-type term, B = 120.7 K is a parameter related to the activation energy, and T_0 = 289.8 K to the onset of segmental mobility associated to an increase of free volume above the glass transition, T_g. We have also fitted the linear region in **Fig. ESI6(a)** (at sufficiently low temperatures) to Arrhenius behaviour, *Eq. (2)*, obtaining an apparent activation energy of E_a = 95 kJ mol^{-1}, Table 2. The range of frequencies are consistent with a Goldstone (phason)-mode, where the molecules rotate within smectic layers without a change in the tilt angle, whilst the higher activation energies may be indicative of cooperative motions [69–71,74]. The confinement of the charged areas would also explain the shift of the relaxation towards higher frequencies, requiring less time to complete than in their non-doped analogue. This assignment is also consistent with the results obtained when superimposing dc fields, **Fig. ESI4(b)**, since ε″ decreases in the relaxation frequency region due to an, at least partial, disruption of the smectic order. Doping has comparable effects on the dielectric responses of Li-TEG-B1-0-14, Fig. 6**(b)**, and its high-frequency relaxation also follows a marked VFT behaviour ($\ln(f_0/Hz)$ = 12.4, B = 259.2 K, T_0 = 267.1 K), with an apparent activation energy of E_a = 105 kJ mol^{-1} in the low-temperature region. A secondary ε″ peak also appears on further cooling below its crystallisation point (T ~ 40 °C), which is

out of practical scope for our discussion. Lastly, the high-frequency response of Li-TEG-Bazo-0-14 undergoes a very weak temperature dependence in Fig. 6**(c)**, and this sample will be studied with more detail in the next section of this manuscript.

Complexation considerably increases the dielectric signal of the doped-materials in the low-frequency region, which is particularly strong for Li-TEG-B1-0-14 and Li-TEG-Bazo-0-14 (in the $\varepsilon'' \sim 1000$ range). As a result, direct current conductivity, σ_{dc}, increases and two plateaus in the double logarithmic σ' vs log(f) plots for these samples appear in Fig. 7, which can be attributed to the presence of ionic charges in the complexes. Even though the σ_{dc} values that can be estimated from Fig. 7**(b) and 7(c)** ($\sigma_{dc} \sim 10^{-5}$ S cm^{-1}) are still much lower than those exhibited by benchmark materials used in energy applications ($\sigma_{dc} \sim 10^{-1}$ S cm^{-1}) [32,75], our results are in the same range as other liquid crystalline electrolytes recently reported and demonstrate the potential of these bent-core materials to develop conductivity [8,43,56,58,76–78]. These results indicate a dual dielectric response of our bent-core materials, in both the short-range, based on the rapid rearrangement of local dipole moments in the bent-cores, and the long-range, sustained on supramolecular organisations.

The moderate σ_{dc} values may be caused by the strong interactions between the TEG chains and the triflate ions illustrated by FT-IR in Fig. 3 and can be explained in the framework of the phase-separated model sketched in Fig. 8, with the lithium and triflate ions located preferentially in the polar segments of the molecules. The occurrence of long-range ionic mobility in the material may be restricted by complexation between the ionic pair and the (–CH_2CH_2O-) chains, which was evidenced by the broadening of the 1300 – 1000 cm^{-1} IR region.

5. Effect of light irradiation on azobenzene-compounds

In line with other reported materials with azobenzene groups [57,79–81], also bent-core type mesogens [51,82,83], TEG-Bazo-0-14 and Li-TEG-Bazo-0-14 possess a light-sensitive character, through *trans-to-cis* photoisomerization of the azobenzene group, see Fig. 9**(a)**, which we have assessed by UV–vis spectrophotometry. We have measured the UV–vis spectra of these compounds in tetrahydrofuran (THF) solutions (~10^{-5} M) at room temperature, before and after light irradiation (h ν) at a frequency of 365 nm (260 mW·cm^{-2}), and in Fig. 9 **(b)** and **Fig. ESI7(a)** we show the results corresponding to TEG-Bazo-0-14 and Li-TEG-Bazo-0-14, respectively. The solutions show one strong band centred at around ~ 365 nm, due to the lowest-energy $\pi^* \leftarrow \pi$ transition in the *trans*-azobenzene isomer, and a secondary absorption peak in the visible region (~440 nm), assigned to a weak $\pi^* \leftarrow n$ transition in the *cis*-azobenzene [79]. Upon UV irradiation, the ~ 365 nm band decreases with a simultaneous (slight) increase of the ~ 440 nm band, which confirms *trans*-to-*cis* photo-induced isomerisation of azobenzene. As expected, when the solutions are kept in the dark after illumination, *cis*-to-*trans* thermal back-relaxation takes place, and the UV–vis spectra recover their initial shape (prior to UV illumination) before 24 h after exposure. The isomerisation kinetics of the solutions are illustrated in Fig. 9**(c)** and **Fig. ESI7(b)**, where we have plotted the maxima of the time-dependent curves, obtaining half-live ($t_{1/2}$) between 4 and 5 h, in the same range of similar bent-core azobenzene-based materials [84]. It is worth mentioning that TEG-Bazo-0-14 and Li-TEG-Bazo-0-14 show comparable UV–visible responses and relaxation times ($t_{1/2} \sim 4.6$ h), which can be explained by the local activation nature of the *trans*-to-*cis* photoisomerization of the azobenzene group in these compounds.

Thus, we have assessed the dielectric and conductivity response of the azobenzene-containing samples under UV light at selected temperatures, according to the procedure described in the experimental section. Light irradiation at 260 mW·cm^{-2} causes some variations in the stripped textures associated to the lamellar organisations of Li-TEG-Bazo-0-14, Fig. 10, but does not suppress its mesomorphism. *Trans*-to-*cis* photoisomerisation of azobenzene units can disrupt the order in liquid crystal phases due to the curved molecular geometry of the *cis*-isomer, compared to the rod-like linear *trans*-isomer [85–88]. Such disruption depends on several factors that regulate the equilibrium between the *trans* and *cis*-isomers, including the irradiation dose, temperature, and also other dynamic effects. At such high temperatures as those reported in Fig. 10 (above 100 °C) we can expect that the thermal relaxation (Δ) may be fast enough to displace the equilibrium towards the recovery of azobenzene *trans*-isomers, and hence the low population of *cis*-isomers may not be sufficient to destabilise the packing order in the bent-core region sketched in Fig. 8.

Light irradiation increases the dielectric loss factor, ε'', and conductivity, σ', of TEG-Bazo-0-14 in the low-frequency range, see Fig. 11**(a) and 11(b)**, respectively, opening the possibility to control the properties of future electrolytes by external stimuli. These effects are particularly prominent at low temperatures, which can have a two-fold explanation. On the one hand, the presence of excited *cis*-molecules may alter to a greater extent the strongly ordered crystal phase in this sample, compared to its isotropic melt. On the other hand, the partial inhibition

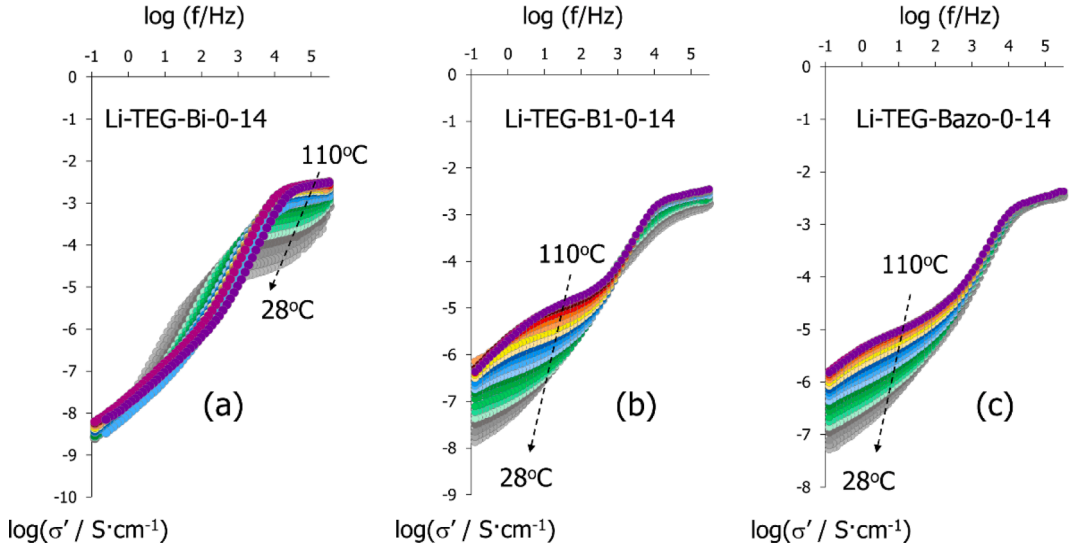

Fig. 7. Double logarithmic plots of the real component of the complex conductivity, σ', measured as a function of the frequency, log(σ') vs log(f), in isothermal steps (°C) on cooling from the isotropic phases for: (a) Li-TEG-Bi-0-14, (b) Li-TEG-B1-0-14, and (c) Li-TEG-Bazo-0-14.

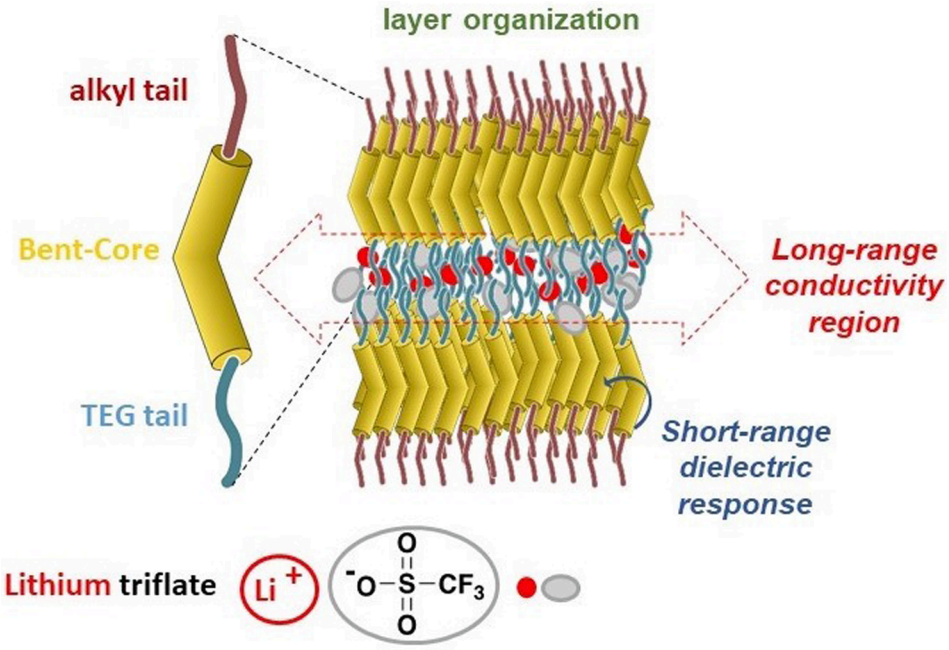

Fig. 8. Schematical model for the formation of non-polar and polar regions within the smectic order and proposed ionic conductivity pathways for the Li-TEG-B*x*-0-14 samples.

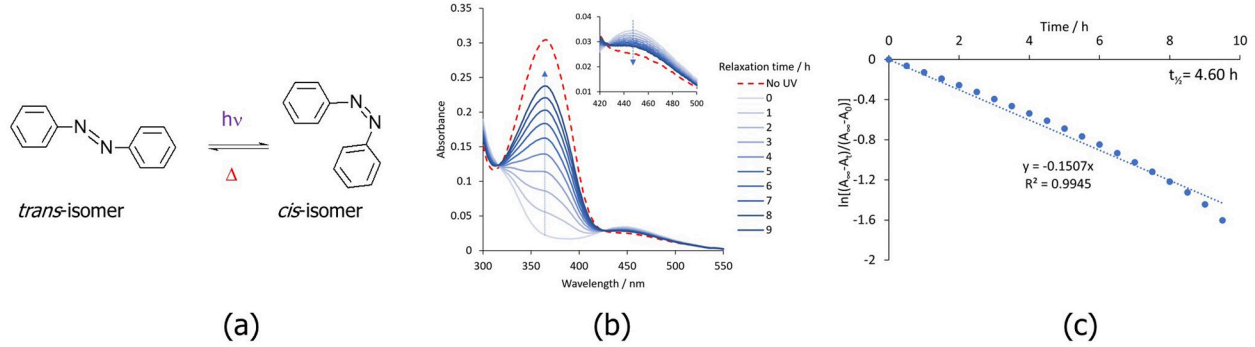

Fig. 9. (a) Representation of the *trans*-to-*cis* photoisomerization of azobenzene groups by light irradiation (h ν), and the reverse *cis*-to-*trans* thermal isomerisation (Δ); (b) UV–visible spectra of TEG-Bazo-0-14 measured before and at different times after light irradiation (260 mW·cm^{-2}; 365 nm, THF 1.3·10^{-5} M solution at room temperature); (c) kinetics of *cis*-to-*trans* (thermal) back-isomerisation obtained using the maximum absorbance values (~365 nm) of the UV–visible spectra in (b) (A_t) after light irradiation (A_0), until the final value is reached (A_∞). Estimation of the half-life times, $t_{1/2}$. Arrows in (b) indicate signal recovery after UV irradiation (t = 0 min) while samples were kept in the dark.

of the thermal relaxation at low temperatures may displace the *trans*-to-*cis* equilibrium towards higher concentrations of *cis*-isomers. Similar effects are observed for Li-TEG-Bazo-0-14, and light irradiation at 40 °C increases the conductivity (σ_{dc}) by one order of magnitude at low frequencies, see Fig. 11**(c)** and **11(d)**. We note, moreover, that UV illumination also causes some slight variations in the high-frequency relaxation process of this sample.

Recently, we observed similar effects on light-responsive bent-core materials, and we hypothesised that the increase in the dielectric and conductivity response can be attributed to slight changes in the smectic microstructure, caused by continuous *trans*-to-*cis*-to-*trans* isomerization processes, which allows for better packaging and molecular alignment [86]. Another possible explanation is the occurrence of *iso*-mesophase micro-transitions (due to isotropisation by the presence of *cis*-isomers), which ultimately favour this alignment.

6. Concluding remarks: potential as energy materials

Two series of bent-core based materials (TEG-B*x*-0-14 and Li-TEG-B*x*-0-14) have been investigated and all of them show dielectric and conductivity response in a broad range of frequencies and temperatures. Doping with lithium triflate promotes microphase separation between the TEG chains, the aromatic cores, and the alkyl tails, which results in the formation of smectic phases. The ion pairs are preferentially solvated at the TEG regions, which results in the dielectric and conductivity processes being confined in (and potentially directed through) 2D lamellar-type domains. Whilst this can be advantageous to control charge transport in electrolytes, it might be necessary to further explore the effect of decoupling the polar segments for each ion in the pair in order to push the conductivity to competitive values, mimicking the behaviour of ionic liquid crystals [43].

Interestingly, the non-doped samples (TEG-B*x*-0-14) also show strong dielectric responses, attributed to changes in the charge distribution across the bent-core molecules in the presence of low electrical fields. We believe that this behaviour must arise from the reorientation of the local dipole existing at the bent rigid cores, which can lead to ferroelectricity in BCLCs [10–18]. Even though the non-doped materials (TEG-B*x*-0-14) do not show mesomorphism (recall Table 1), we have

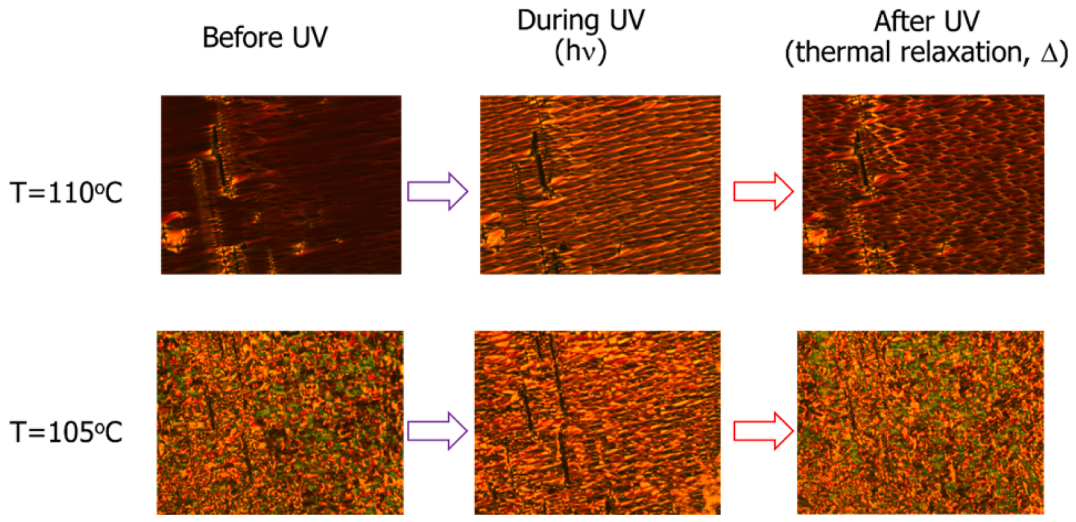

Fig. 10. Polarised optical micrographs of Li-TEG-Bazo-0-14 obtained before (left column), during (central column) and after (right column) UV irradiation (365 nm, 260 mW·cm^{-2}).

carried out triangular hysteresis loops on these samples in their crystal phases, applying different (and slightly stronger than 1 V_{rms}) electrical fields. The three bent-core compounds of the series exhibit non-linear polarisation response in solid phase, and remanent polarisation (at zero voltage, P_r), typical of ferroelectric behaviour, see Fig. 12 and **Fig. ESI8**. Ferroelectricity in our bent-core compounds must be then driven by the reorientation of the molecular dipoles within crystalline domains, which remain locked after their removal due to steric constrains. The occurrence of molecular reorientations in the crystal phase is consistent with the low activation energies displayed in Table 2 for the non-doped materials.

Whist the saturation polarisation values, P_s, are comparable to other bent-core based materials, [13,15,89,90] the low remanent polarisation values, P_r, reached when the fields are removed can denote relaxor behaviour [91,92]. This difference between P_s and P_r can be attributed to the potential of these materials to store energy, E_S, which can be associated to the shadowed area in Fig. 12, illustrated for TEG-Bazo-0-14, with estimated values in the 1.62 to 1.65 mJ cm^{-3} range for the three compounds (comparable to those obtained in our previous work on other BLCS [86]).

As a comparative analysis on the impact of the incorporation of three different lateral molecular structures (B1, Bi and Bazo), specifically on materials doped with Li triflate, it can be highlighted that:

- Its effect on the liquid crystal properties is mainly reflected in the type and range of organization in the mesophase, SmCP in the case of B1, and more a complex on (HNF-like) in the case of Bi and Bazo. However, although in ITO cells the Bi and Bazo structures stabilize the mesophase at higher temperatures (above 150 °C) compared to 130 °C for B1, the differences in molecular organization seem to disappear due to surface effects.

- The dielectric response is comparable in the three non-doped materials, probably due to the prominence of the ester dipoles (–COO-) to the dielectric properties in the short molecular range, and the high-frequency response does not differ very much after complexation either (within different (B1, Bi and Bazo lateral structures).

- After complexation, both the B1 and Bazo structures in the bent-cores seem to promote higher long-range conductivities (low-frequency end) than the biphenyl (Bi) analogue. We speculate with the higher polarity of the former groups, which may assist phase separation and promote ionic conductivity localized in the ethylene-oxide regions.

Lastly, we have also proved that light irradiation can enhance the dielectric response and conductivity of the bent-core compounds containing azobenzene groups, via *trans*-to-*cis* photoisomerisation. This happens by disrupting the local order of either crystal (TEG-Bazo-0-14) or liquid crystal (Li-TEG-Bazo-0-14) phases. These results are promising to exert physical control over the dielectric response of new electrolytes, which can be applied in energy conversion and storage applications. For example, similar principles can be used in new photosensors triggered by light-induced conductivity, or in energy storage electrolytes, if the excited states induced by light irradiation can be stabilised during longer times after exposure [93].

Future and more profound analyses on Li-TEG-Bazo-0-14 and further related materials are required to rationalise the combination of effects on the conductivity, including, temperature, light-intensity, efficiency, and kinetics of *trans*-to-*cis* photoisomerisation and subsequent *cis*-to-*trans* thermal relaxation. These and other factors are the object ongoing work using transient and steady state UV investigations. We will also consider different salt-to-bent-core ratio and anion structure effect, to assess the effect of composition on the transitional properties and dielectric response of new bent-core liquid crystal electrolytes.

7. Funding Sources

AMF would like to thank the Carnegie Trust for the Universities of Scotland, for the Research Incentive Grant RIG008586, the Royal Society and Specac Ltd., for the Research Grant RGS\R1\201397, the Royal Society of Chemistry for the award of a mobility grant (M19-0000), and the Scottish Government and the Royal Society of Edinburgh for the award of a SAPHIRE project. JP would like to acknowledge the School of Engineering at the University of Aberdeen, for the award of an undergraduate research summer scholarship. The authors from INMA greatly appreciate the Spanish Government project PID2021-122882NB-I00 funded by MCIN/AEI /10.13039/501100011033/ and by FEDER - *Una manera de hacer Europa*; the Gobierno de Aragón/FEDER (research group E47_23R) and BES-2016-078753 MINECO-FEDER (M. C.-V.) fellowship programs for support. These authors would like to acknowledge the nuclear magnetic resonance, mass spectrometry, and thermal analysis services of CEQMA (Univ. Zaragoza-CSIC), the LMA (Univ. Zaragoza) for TEM equipment and the use of Servicio General de Apoyo a la Investigación-SAI, Universidad de Zaragoza. NFKA would like to thank Universiti Teknologi MARA (UiTM) for sponsoring her academic sabbatical leave and allowing her to work on this project.

8. Author statement

During the preparation of this work the authors did not use AI for

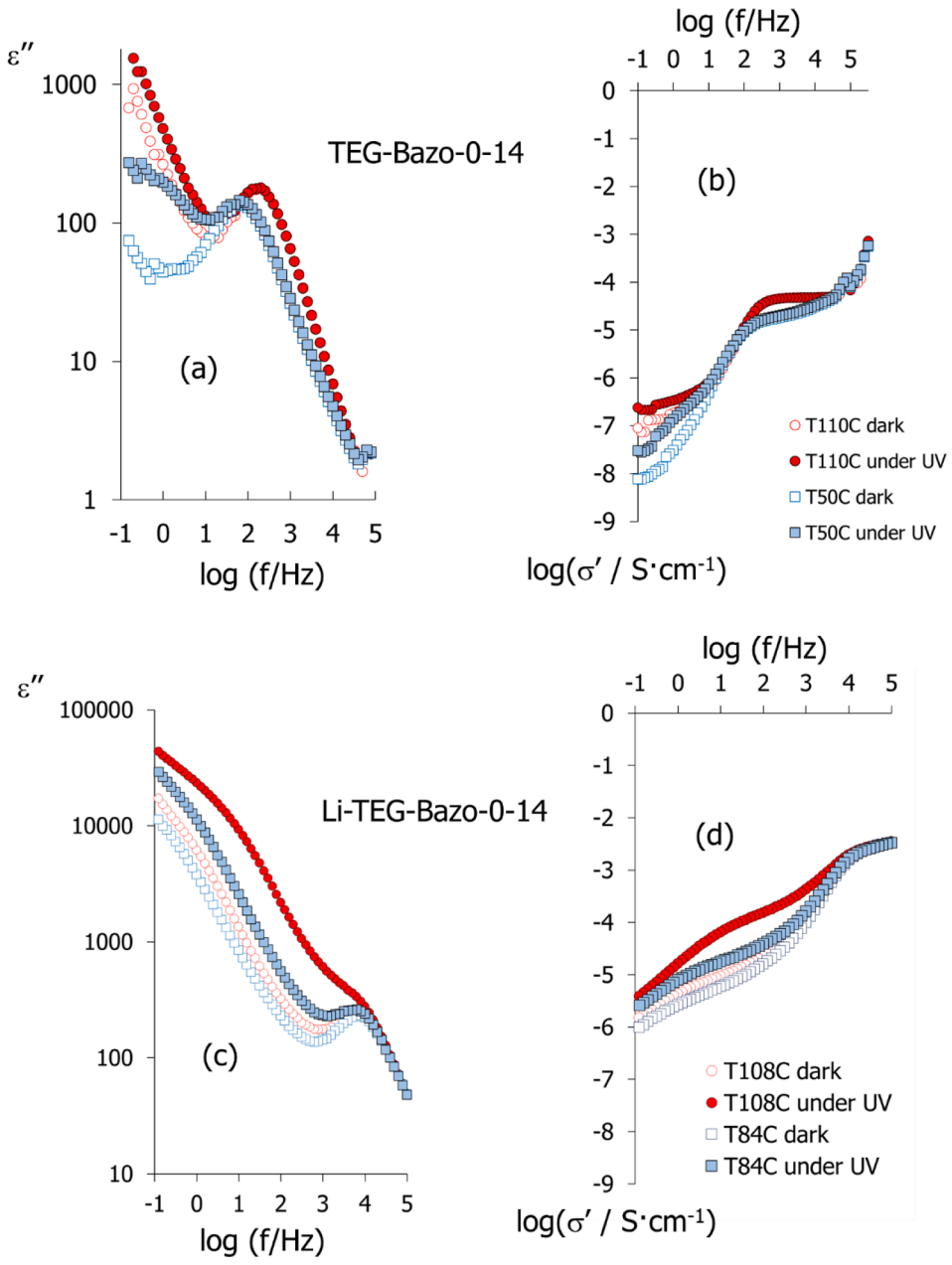

Fig. 11. Effect of UV irradiation (250 mW·cm^{-2}) on the dielectric loss factor, ε″ (graphs a, c) and conductivity, σ′ (b, d) of TEG-Bazo-0-14 and Li-TEG-Bazo-0-14.

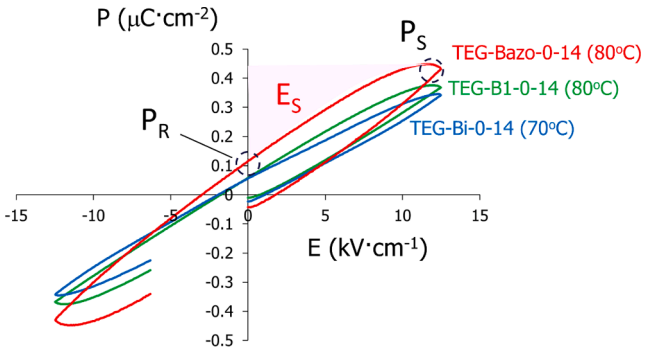

Fig. 12. Hysteresis loops demonstrating the ferroelectric response of the TEG-Bx-0-14 samples in their crystal phase, under 10 Hz and ±10 V_{rms} fields, showing the remanent polarisation, P_R, saturated polarisation, P_S, and the energy stored, E_S, associated to the shadowed area.

writing or assessing the text.

CRediT authorship contribution statement

Alfonso Martinez-Felipe: Conceptualization, Funding acquisition, Supervision, Writing – original draft, Writing – review & editing. **Daniel Zaton:** Investigation, Methodology, Formal analysis. **Martín Castillo-Vallés:** Investigation, Methodology. **Asia Baldini:** Investigation, Data curation, Formal analysis. **Jonathan Pease:** Investigation, Methodology, Data curation, Formal analysis. **Natalie Leader:** Data curation, Formal analysis. **Nurul Fadhilah Kamalul Aripin:** Funding acquisition, Investigation, Methodology. **Marco Giacinti-Baschetti:** Supervision, Project management. **M. Blanca Ros:** Conceptualization, Funding acquisition, Supervision, Writing – original draft, Writing – review & editing.

Declaration of Competing Interest

The authors declare the following financial interests/personal relationships which may be considered as potential competing interests: Alfonso Martinez-Felipe reports financial support was provided by Carnegie Trust for the Universities of Scotland. Alfonso Martinez-Felipe reports financial support was provided by The Royal Society. Alfonso Martinez-Felipe reports financial support was provided by Royal Society of Chemistry. Alfonso Martinez-Felipe reports financial support was provided by Royal Society of Edinburgh. Blanca Ros reports financial support was provided by Spanish Government. M. Blanca Ros reports financial support was provided by Gobierno de Aragón.

Data availability

Data will be made available on request.

Acknowledgements

AMF would like to thank Ivan Dominguez-Candela for his support during the ferroelectric measurements.

Appendix A. Supplementary data

Supplementary data to this article can be found online at https://doi.org/10.1016/j.molliq.2023.123100.

References

[1] E.C. Pereira, A. Cuesta, A personal perspective on the role of electrochemical science and technology in solving the challenges faced by modern societies, J. Electroanal. Chem. 780 (2016) 355–359.
[2] P.K. Bhowmik, Dicationic Ionic Liquids based on Bis(4-oligoethyleneoxyphenyl) Viologen Bistriflimide Salts Exhibiting High Ionic Conductivities, J. Mol. Liq. (2022).
[3] A. Martinez-Felipe, Liquid crystal polymers and ionomers for membrane applications, Liq. Cryst. 38 (11–12) (2011) 1607–1626.
[4] T. Kato, et al., Functional Liquid Crystals towards the Next Generation of Materials, Angew. Chem.-Int. Ed. 57 (16) (2018) 4355–4371.
[5] J. Uchida, et al., Advanced Functional Liquid Crystals, Adv. Mater. 34 (2022) 23.
[6] T. Kato, et al., Transport of ions and electrons in nanostructured liquid crystals, Nat. Rev. Mater. 2 (4) (2017) 17001.
[7] A. Pipertzis, et al., Ionic Conduction in Poly(ethylene glycol)-Functionalized Hexa-peri-hexabenzocoronene Amphiphiles, Macromolecules 50 (5) (2017) 1981–1990.
[8] B.K. Cho, Nanostructured organic electrolytes, RSC Adv. 4 (1) (2014) 395–405.
[9] D.A. Dunmur, et al., Dielectric studies of liquid crystals: the influence of molecular shape, Liq. Cryst. 37 (6–7) (2010) 723–736.
[10] R.A. Reddy, C. Tschierske, Bent-core liquid crystals: polar order, superstructural chirality and spontaneous desymmetrisation in soft matter systems, J. Mater. Chem. 16 (10) (2006) 907–961.
[11] H. Takezoe, Y. Takanishi, Bent-core liquid crystals: Their mysterious and attractive world, Japan. J. Appl. Phys. Part 1-Regular Papers Brief Communications & Review Papers 45 (2A) (2006) 597–625.
[12] C. Tschierske, Development of Structural Complexity by Liquid-Crystal Self-assembly, Angew. Chem.-Int. Ed. 52 (34) (2013) 8828–8878.
[13] A. Eremin, A. Jakli, Polar bent-shape liquid crystals - from molecular bend to layer splay and chirality, Soft Matter 9 (3) (2013) 615–637.
[14] H. Takezoe, A. Eremin, *Bent-Shaped Liquid Crystals: Structures and Physical Properties.* Bent-Shaped Liquid Crystals: Structures and Physical Properties, 2017.
[15] H. Takezoe, Polar liquid crystals - ferro, antiferro, banana, and columnar, Mol. Cryst. Liq. Cryst. 646 (1) (2017) 46–65.
[16] K.V. Le, H. Takezoe, F. Araoka, Chiral Superstructure Mesophases of Achiral Bent-Shaped Molecules - Hierarchical Chirality Amplification and Physical Properties, Adv. Mater. 29 (25) (2017) 1602737.
[17] T. Niori, et al., Distinct ferroelectric smectic liquid crystals consisting of banana shaped achiral molecules, J. Mater. Chem. 6 (7) (1996) 1231–1233.
[18] J. Etxebarria, M.B. Ros, Bent-core liquid crystals in the route to functional materials, J. Mater. Chem. 18 (25) (2008) 2919–2926.
[19] D. Chen, et al., Chiral Isotropic Sponge Phase of Hexatic Smectic Layers of Achiral Molecules, ChemPhysChem 15 (7) (2014) 1502–1507.
[20] A. Jakli, et al., Helical filamentary growth in liquid crystals consisting of banana-shaped molecules, Liq. Cryst. 27 (11) (2000) 1405–1409.
[21] R. Meyer, in: R. Balian, G. Weil (Eds.), Molecular Fluids, Gordon and Breach, New York, 1976, pp. 273–373.
[22] M. Cestari, et al., Phase behavior and properties of the liquid-crystal dimer 1 “,7 ”-bis(4-cyanobiphenyl-4 ’- yl) heptane: A twist-bend nematic liquid crystal, Phys. Rev. E 84 (3) (2011), 031704.
[23] I. Dozov, On the spontaneous symmetry breaking in the mesophases of achiral banana-shaped molecules, Europhys. Lett. 56 (2) (2001) 247–253.
[24] R.J. Mandle, S.J. Cowling, J.W. Goodby, A nematic to nematic transformation exhibited by a rod-like liquid crystal, PCCP 19 (18) (2017) 11429–11435.
[25] A. Mertelj, et al., Splay Nematic Phase, Phys. Rev. X 8 (2018) 4.
[26] N. Sebastian, et al., Ferroelectric-Ferroelastic Phase Transition in a Nematic Liquid Crystal, Phys. Rev. Lett. 124 (3) (2020), 037801.
[27] H. Nishikawa, et al., A Fluid Liquid-Crystal Material with Highly Polar Order, Adv. Mater. 29 (43) (2017) 1702354.
[28] M. Castillo-Vallés, et al., Self-assembly of bent-core amphiphiles joining the ethylene-oxide/lithium ion tandem, J. Mol. Liq. 381 (2023), 121825.
[29] Q.H. Zeng, et al., Semi-interpenetrating-network all-solid-state polymer electrolyte with liquid crystal constructing efficient ion transport channels for flexible solid lithium-metal batteries, J. Energy Chem. 67 (2022) 157–167.
[30] J.D. Hwang, et al., Effect of Noncovalent Dispersion of Poly(Ethylene Oxide) in Columnar Polyether-Based Discotic Liquid Crystal on the Ionic Conductivity and Dynamics of Lithium Ions, Crystals 9 (12) (2019) 627.
[31] P. Judeinstein, F. Roussel, Ionic conductivity of lithium salt/oligo (ethylene oxide)-based liquid-crystal mixtures: The effect of molecular architecture on the conduction process, Adv. Mater. 17 (6) (2005) p. 723.
[32] A.C. Luntz, B.D. McCloskey, Nonaqueous Li-Air Batteries: A Status Report, Chem. Rev. 114 (23) (2014) 11721–11750.
[33] Z. Stoeva, et al., A new polymer electrolyte based on a discotic liquid crystal triblock copolymer, Electrochim. Acta 93 (2013) 279–286.
[34] Y.F. Tong, et al., Mesogen-Controlled Ion Channel of Star-Shaped Hard-Soft Block Copolymers for Solid-State Lithium-Ion Battery, J. Polym. Sci. Part a-Polymer Chem. 51 (20) (2013) 4341–4350.
[35] Y.F. Tong, et al., Free Mesogen Assisted Assembly of the Star-shaped Liquid-crystalline Copolymer/Polyethylene Oxide Solid Electrolytes for Lithium Ion Batteries, Electrochim. Acta 118 (2014) 33–40.
[36] S. Wang, et al., High-Performance All-Solid-State Polymer Electrolyte with Controllable Conductivity Pathway Formed by Self-Assembly of Reactive Discogen and Immobilized via a Facile Photopolymerization for a Lithium-Ion Battery, ACS Appl. Mater. Interfaces 10 (30) (2018) 25273–25284.
[37] S. Wang, et al., An ionic liquid crystal-based solid polymer electrolyte with desirable ion-conducting channels for superior performance ambient-temperature lithium batteries, Polym. Chem. 9 (37) (2018) 4674–4682.
[38] S. Wang, et al., Six-arm star polymer based on discotic liquid crystal as high performance all-solid-state polymer electrolyte for lithium-ion batteries, J. Power Sources 395 (2018) 137–147.
[39] M. Zhang, et al., Conductivity of PEO/PLA Doped Liquid Crystal Ionomer Solid Polymer Electrolyte in Mesomorphic Range, J. Polym. Environ. 27 (11) (2019) 2369–2379.
[40] A. Kuwabara, et al., Nanostructured liquid-crystalline Li-ion conductors with high oxidation resistance: molecular design strategy towards safe and high-voltage-operation Li-ion batteries, Chem. Sci. 11 (39) (2020) 10631–10637.
[41] T. Onuma, et al., Noncovalent Approach to Liquid-Crystalline Ion Conductors: High-Rate Performances and Room-Temperature Operation for Li-Ion Batteries, ACS Omega 3 (1) (2018) 159–166.
[42] J. Sakuda, et al., 2D assemblies of ionic liquid crystals based on imidazolium moieties: formation of ion-conductive layers, New J. Chem. 39 (6) (2015) 4471–4477.
[43] P.K. Bhowmik, et al., Ionic liquid crystals: Synthesis and characterization via NMR, DSC, POM, X-ray diffraction and ionic conductivity of asymmetric viologen bistriflimide salts, J. Mol. Liq. 328 (2021), 115370-115370.
[44] M.A. Kolmangadi, et al., Side Chain Length-Dependent Dynamics and Conductivity in Self-Assembled Ion Channels, J. Phys. Chem. C 126 (2022) 10995–11006.
[45] M.A. Kolmangadi, et al., Side Chain Length-Dependent Dynamics and Conductivity in Self- Assembled Ion Channels, J. Phys. Chem. C 126 (27) (2022) 10995–11006.
[46] R. Forschner, et al., Luminescent liquid crystals: from supramolecular plant dyes to emissive flavylium salts, Liq. Cryst. (2023), https://doi.org/10.1080/02678292.2023.2179122.
[47] A. Nafees, G. Kalita, A. Sinha, Effect of titanium dioxide nanoparticles on the dielectric and electro-optical properties of bent-core liquid crystals, J. Mol. Liq. 274 (2019) 592–597.
[48] A. Jakli, et al., Light-induced changes of optical and electrical properties in bent-core azo compounds, Phys. Rev. E 71 (2) (2005), 021709.
[49] J. Heuer, et al., Longitudinal and normal electroconvection rolls in a nematic liquid crystal with positive dielectric and negative conductivity anisotropy, Phys. Rev. E 77 (5) (2008) 056206.
[50] A.K. Srivastava, et al., Anomalously high dielectric strength and low frequency dielectric relaxation of a bent-core liquid crystal with a large kink angle, Curr. Appl Phys. 17 (6) (2017) 858–863.
[51] M. Alaasar, Azobenzene-containing bent-core liquid crystals: an overview, Liq. Cryst. 43 (13–15) (2016) 2208–2243.
[52] R. Sumitani, H. Yoshikawa, T. Mochida, Reversible control of ionic conductivity and viscoelasticity of organometallic ionic liquids by application of light and heat, Chem. Commun. 56 (46) (2020) 6189–6192.
[53] C. Tonnele, et al., Atomistic simulations of charge transport in photoswitchable organic-graphene hybrids, J. Phys.-Mater. 2 (3) (2019), 035001.
[54] J.Y. Park, U. Male, D.S. Huh, Photo-regulated conductivity of polycaprolactone honeycomb-patterned porous films containing azobenzene-functionalized reduced graphene oxide, Macromol. Res. 25 (8) (2017) 849–855.
[55] B. Soberats, et al., Macroscopic Photocontrol of Ion-Transporting Pathways of a Nanostructured Imidazolium-Based Photoresponsive Liquid Crystal, J. Am. Chem. Soc. 136 (27) (2014) 9552–9555.

[56] S.M. Alauddin, et al., New side-chain liquid crystalline terpolymers with anhydrous conductivity: Effect of azobenzene substitution on light response and charge transfer, Eur. Polym. J. 146 (2021), 110246–110246.
[57] T.S. Velayutham, et al., A new light-responsive resistive random-access memory device containing hydrogen-bonded complexes, J. Photochem. Photobiol. A Chem. 404 (2021) 112914.
[58] S. Mohd Alauddin, et al., Liquid Crystalline Copolymers Containing Sulfonic and Light-Responsive Groups: From Molecular Design to Conductivity, Molecules 25 (11) (2020) 2579.
[59] S.M. Alauddin, et al., The role of conductivity and molecular mobility on the photoanisotropic response of a new azo-polymer containing sulfonic, groups 389 (2020) 112268.
[60] D. Chen, et al., Structure of the B4 Liquid Crystal Phase near a Glass Surface, ChemPhysChem 13 (1) (2012) 155–159.
[61] A. Martinez-Felipe, C.T. Imrie, A. Ribes-Greus, Study of Structure Formation in Side-Chain Liquid Crystal Copolymers by Variable Temperature Fourier Transform Infrared Spectroscopy, Ind. Eng. Chem. Res. 52 (26) (2013) 8714–8721.
[62] A.G. Bishop, et al., Triflate ion association in plasticized polymer electrolytes, Solid State Ion. 85 (1–4) (1996) 129–135.
[63] A.G. Bishop, et al., FT-IR investigation of ion association in plasticized solid polymer electrolytes, J. Phys. Chem. 100 (6) (1996) 2237–2243.
[64] S.P. Gejji, et al., Geometry and vibrational frequencies of the lithium triflate ion-pair - An ab-initio study,, J. Phys. Chem. 97 (44) (1993) 11402–11407.
[65] J. Stygar, G. Zukowska, W. Wieczorek, Study of association in alkali metal perchlorate-poly(ethylene glycol) monomethyl ether solutions by FT-IR spectroscopy and conductivity measurements, Solid State Ion. 176 (35–36) (2005) 2645–2652.
[66] C. Tschierske, Microsegregation: From Basic Concepts to Complexity in Liquid Crystal Self-Assembly, Isr. J. Chem. 52 (10) (2012) 935–959.
[67] A. Martinez-Felipe, et al., Characterization of Functionalized Side-Chain Liquid Crystal Methacrylates Containing Nonmesogenic Units by Dielectric Spectroscopy, Ind. Eng. Chem. Res. 52 (26) (2013) 8722–8731.
[68] A.W. Brown, A. Martinez-Felipe, Ionic conductivity mediated by hydrogen bonding in liquid crystalline 4-n-alkoxybenzoic acids, J. Mol. Struct. 1197 (2019) 487–496.
[69] L. Guo, et al., Transition between two orthogonal polar phases in symmetric bent-core liquid crystals, Soft Matter 7 (6) (2011) 2895–2899.
[70] L.F. Guo, et al., Ferroelectric behavior of orthogonal smectic phase made of bent-core molecules, Phys. Rev. E 84 (3) (2011).
[71] F. Gouda, K. Skarp, S.T. Lagerwall, Dielectric studies of the soft mode and Goldstone mode in ferroelectric liquid crystals, Ferroelectrics 113 (1) (1991) 165–206.
[72] J.C. Dyre, Some remarks on ac conduction in disordered solids, J. Non Cryst. Solids 135 (2–3) (1991) 219–226.
[73] C.A. Angell, C.T. Imrie, M.D. Ingram, From simple electrolyte solutions through polymer electrolytes to superionic rubbers: Some fundamental considerations, Polym. Int. 47 (1) (1998) 9–15.
[74] S.U. Vallerien, et al., Field-Dependent Soft and Goldstone Mode in a Ferroelectric Liquid-Crystal as Studied by Dielectric-Spectroscopy, Phys. Lett. A 138 (4–5) (1989) 219–222.
[75] K.A. Mauritz, R.B. Moore, State of understanding of Nafion, Chem. Rev. 104 (10) (2004) 4535–4585.
[76] A. Concellon, et al., Proton conductive ionic liquid crystalline poly(ethyleneimine) polymers functionalized with oxadiazole, RSC Adv. 8 (66) (2018) 37700–37706.
[77] J.S. Yang, et al., New anhydrous proton exchange membranes based on fluoropolymers blend imidazolium poly (aromatic ether ketonejs for high temperature polymer electrolyte fuel cells, Int. J. Hydrogen Energy 43 (17) (2018) 8464–8473.
[78] T. Liang, et al., Anisotropic Dye Adsorption and Anhydrous Proton Conductivity in Smectic Liquid Crystal Networks: The Role of Cross-Link Density, Order, and Orientation, ACS Appl. Mater. Interfaces 9 (40) (2017) 35218–35225.
[79] G.S. Kumar, D.C. Neckers, Photochemistry of Azobenzene-Containing Polymers, Chem. Rev. 89 (8) (1989) 1915–1925.
[80] G. Hegde, et al., Synthesis and liquid crystalline behaviour of substituted (E)-phenyl-4-(phenyldiazenyl) benzoate derivatives and their photo switching ability, Liq. Cryst. 43 (11) (2016) 1578–1588.
[81] B.N. Sunil, et al., Influence of inter- and intramolecular H-bonding on the mesomorphic and photoswitching behaviour of (E)-4-((4-(hexyloxy)phenyl) diazenyl)-N-phenyl benzamides, RSC Adv. 10 (34) (2020) 20222–20230.
[82] B.S. Ranjitha, et al., Impact of terminal group on azobenzene liquid crystal dimers for photo-responsive optical storage devices, J. Mol. Liq. 383 (2023), 121985.
[83] B.N. Sunil, et al., Effective tuning of optical storage devices using photosensitive bent-core liquid crystals, J. Mol. Liq. 304 (2020) 112719.
[84] I. Chaganava, et al., Induction of the vector polyphotochromism in side-chain azopolymers, J. Photochem. Photobiol. A-Chem. 354 (2018) 70–77.
[85] D. Zaton, et al., Photo-driven effects in twist-bend nematic phases: Dynamic and memory response of liquid crystalline dimers, J. Mol. Liq. 344 (2021), 117680.
[86] I. Dominguez-Candela, et al., Light-responsive bent-core liquid crystals as candidates for energy conversion and storage, J. Mater. Chem. C 10 (48) (2022) 18200–18212.
[87] S.K. Prasad, et al., A soft-bent dimer composite exhibiting twist-bend nematic phase: Photo-driven effects and an optical memory device, Appl. Phys. Lett. 112 (25) (2018) 253701.
[88] S.K. Prasad, et al., Photoinduced effects in nematic liquid crystals, Phase Transit. 78 (6) (2005) 443–455.
[89] W. Weissflog, et al., In search of a new design strategy for solid single-component organic ferroelectrics: Polar crystalline phases formed by bent-core molecules, J. Mater. Chem. 20 (29) (2010) 6057–6079.
[90] A. Jakli, Liquid crystals of the twenty-first century - nematic phase of bent-core molecules, Liq. Cryst. Rev. 1 (1) (2013) 65–82.
[91] M.M. El-Desoky, et al., Relaxor ferroelectric-like behavior in 10PbTiO(3)-10Fe(2)O(3)-30V(2)O(5)-50B(2)O(3) glass for energy storage applications, J. Mater. Sci.-Mater. Electron. 32 (17) (2021) 22408–22416.
[92] W.J. Shi, et al., Relaxor antiferroelectric-like characteristic boosting enhanced energy storage performance in eco-friendly (Bi0.5Na0.5)TiO3-based ceramics, J. Eur. Ceram. Soc. 42 (11) (2022) 4528–4538.
[93] A.R. Ibrahim, et al., p-Methoxy Azobenzene Terpolymer as a Promising Energy-Storage Liquid Crystal System, J. Phys. Chem. C 125 (41) (2021) 22472–22482.